Internal Report ITeSRE/CNR 269/2000

March 2000

EFFECTS OF INSTRUMENTAL NOISE AND OPTICAL DISTORTIONS ON PLANCK LFI OBSERVATIONS

C. Burigana[1], D. Maino[2], N.Mandolesi[1], M.Bersanelli[3], M. Maltoni[4,5], L. Valenziano[1], F. Villa[1], K.M. Górski[6], B.D. Wandelt[7], E. Hivon[8] & A. Banday[9]

[1] *Istituto TeSRE, Consiglio Nazionale delle Ricerche, Via Gobetti 101, I-40129 Bologna, Italy*
[2] *SISSA, International School for Advanced Studies, Via Beirut 2-4, I-34014 Trieste, Italy*
[3] *IFC, Consiglio Nazionale delle Ricerche, Via Bassini 15, I-20133 Milano, Italy*
[4] *Instituto de Física Corpuscular - C.S.I.C., Departament de Física Teòrica, Universitat de València, Edificio Institutos de Paterna, Apt. 2085, E-46071 Valencia, Spain*
[5] *INFN, Sezione di Ferrara, Via Paradiso 12, I-44100 Ferrara, Italy*
[6] *ESO, European Southern Observatory, Karl-Schwarzschild Str. 2, D-85748, Garching, Germany*
[7] *TAC, Theoretical Astrophysics Center, Juliane Maries Vej 30, DK-2100 Copenhagen, Denmark*
[8] *CalTech, California Institute of Technology, 1200 East California Boulevard, CA-91125 Pasadena, USA*
[9] *MPA, Max Planck Inst. für Astrophysik, Karl-Schwarzschild Str. 1, D-85740, Garching, Germany*

Internal Report ITeSRE/CNR 269/2000

March 2000

EFFECTS OF INSTRUMENTAL NOISE AND OPTICAL DISTORTIONS ON PLANCK LFI OBSERVATIONS

C. Burigana[1], D. Maino[2], N.Mandolesi[1], M.Bersanelli[3], M. Maltoni[4,5], L. Valenziano[1], F. Villa[1], K.M. Górski[6], B.D. Wandelt[7], E. Hivon[8] & A. Banday[9]

[1] *Istituto TeSRE, Consiglio Nazionale delle Ricerche, Via Gobetti 101, I-40129 Bologna, Italy*

[2] *SISSA, International School for Advanced Studies, Via Beirut 2-4, I-34014 Trieste, Italy*

[3] *IFC, Consiglio Nazionale delle Ricerche, Via Bassini 15, I-20133 Milano, Italy*

[4] *Instituto de Física Corpuscular - C.S.I.C., Departament de Física Teòrica, Universitat de València, Edificio Institutos de Paterna, Apt. 2085, E-46071 Valencia, Spain*

[5] *INFN, Sezione di Ferrara, Via Paradiso 12, I-44100 Ferrara, Italy*

[6] *ESO, European Southern Observatory, Karl-Schwarzschild Str. 2, D-85748, Garching, Germany*

[7] *TAC, Theoretical Astrophysics Center, Juliane Maries Vej 30, DK-2100 Copenhagen, Denmark*

[8] *CalTech, California Institute of Technology, 1200 East California Boulevard, CA-91125 Pasadena, USA*

[9] *MPA, Max Planck Inst. für Astrophysik, Karl-Schwarzschild Str. 1, D-85740, Garching, Germany*

SUMMARY – The impact of three classes of instrumental effects on Planck Low Frequency Instrument (LFI) observations has been discussed. The first, the so called 1/f noise is related to the LFI receivers; the other two, main beam distortions and Galaxy straylight are related to the optical properties of the Planck telescope, feed horn design and focal plane unit (FPU) configuration. We have simulated Planck/LFI observations in presence of these effects, obtaining data steams for different scanning strategies. The data streams and the derived maps have been analysed using different "quality" estimators: maximum and average contamination of the data streams and sky maps, rms added noise, Fourier decomposition of scan circle data and angular power spectrum recovering. The instrumental effects have been analysed for different ranges of multipoles for comparison with those introduced by the main sources of astrophysical contamination.

1 Introduction

Many sources of systematic effects may be in principle crucial for Planck LFI observations.

We focus here on the impact of three classes of instrumental effects, the first, the so called $1/f$ noise, related to Planck LFI receivers, the other two, main beam distortions and Galaxy straylight, related to the optical properties of the Planck telescope, feed horn design and FPU configuration.

We present here the main results from our simulation work and compare the relative weight of these three classes of systematic effects as well as their impact with that introduced by astrophysical contamination.

2 The $1/f$ noise

The $1/f$, or low-frequency, noise generated by LFI InP HEMT amplifier gain instabilities (Gaier et al. 1996), is particularly relevant for the LFI radiometers, leading to stripes in the final maps which increase the overall noise level and may alter the statistical analysis of the anisotropy distribution. The LFI radiometer design (a pseudo-correlation receiver with a reference load at a temperature of 4 K) has been choosen specifically to minimize the effect of $1/f$ gain fluctuations. Nonetheless, residual striping may be present, and we have studied how to reduce their effect.

The analytical work by Seiffert et al. (1997) has shown the dependency of the $1/f$ noise upon the radiometer characteristics such as the bandwidth, the noise temperature, payload environment temperature and other quantities properly related to Planck LFI radiometers. They can be combined to define a representative parameter, the "knee-frequency" f_k, which has to be kept as low as possible compared with the spinning frequency f_s of the spacecraft. Janssen et al. (1996) have indeed demonstrated that for $f_k \gtrsim f_s$ a degradation in final sensitivity will result.

With the current instrument specifications (Mandolesi et al. 1998) typical theoretical "optimistic" values of the knee-frequency are $f_k = 0.046$ Hz and $f_k = 0.11$ Hz at 30 and 100 GHz respectively with a 20 K load. Lower values of f_k can be reached by lowering the load temperature possibly up to values ($\simeq 4$ K) close to the full (sky plus environment) signal entering the horn (Seiffert et al. 1997). A value as low as $f_k \sim 0.01$ Hz at 100 GHz has been measured by M. Seiffert (1999) with the JPL experimental radiometric assembly (see the "LFI Design Report" of Planck LFI, ISVR, 1999).

We have the possibility to generate different kinds of noise spectra by working in Fourier space and generate the real and imaginary part of Fourier coefficients of our noise signal with appropriate spectrum and FFT (Fast Fourier Transform; Cooley & Tukey 1965; Heideman et al. 1984) them to obtain a real noise stream which has to be normalized to the white noise level. This noise stream can be put in a flight simulation code to quantify the impact of $1/f$ noise in Planck observations in absence of algorithms able to reduce its impact. By coadding the simulated data streams we can obtain a simulated observed map of the instrumental noise. The evaluation of the angular power spectrum, C_ℓ, is a standard way for a quantitative analysis. This is shown in Fig. 1 for a typical LFI beam at 30 GHz in terms of $\delta T_\ell = \sqrt{\ell(2\ell+1)C_\ell/4\pi}$.

As reported by Janssen et al. (1996) the effect of $1/f$ noise can be seen as one or more additive levels, different for each scan circle. To remove these additive levels and "clean" the "observed" map we have then implemented a destriping code (Bersanelli et al. 1996) based on the global minimization of the differences between the temperatures measured at

the same sky positions in different scan circles. This allow us to quantify the impact of $1/f$ noise after applying our destriping algorithm for a large set of scanning strategies, with angles $70° \leq \alpha \leq 90°$ between the telescope optical axis and the satellite spin axis, with different repointing schemes (e.g., moving the spin axis always on the ecliptic plane or by allowing for oscillations over the ecliptic, neglecting thermal drifts), beam locations on the Planck telescope sky field of view (e.g. in polar coordinates θ_B, ϕ_B) and knee frequencies. Our flight simulator and destriping code as well as the main results for the $1/f$ noise and their implications are extensively presented in Burigana et al. (1997) and Maino et al. (1999); the efficiency of the destriping technique has been there quantified by using estimators such as χ^2 or the rms temperature of the stripes, and by studying the impact of the $1/f$ noise on the CMB power spectrum reconstruction. Fig. 2 shows the receiver noise angular power spectrum after applying our destriping code for the same parameters of Fig. 1.

Table 1 summarize our results at 30 GHz for a suitable set of scanning strategies and beam location: we show the averaged module of the residual (i.e. after having applied the destriping algorithm) relative increase of the square root of the noise angular power spectrum with respect to the case of a simulation with pure white noise for three ranges of multipoles, $\ell \leq 200$, $\ell \geq 200$ and for the whole range of ℓ (we limit ourselves to $\ell \lesssim 500$, approximately corresponding to the angular resolution at 30 GHz).

Configuration	$\ell \leq 200$	$\ell \geq 200$	all ℓ
$\alpha = 90°$, off-axis beam	19.3%	3.5%	9.7%
$\alpha = 90°$, off-axis beam + prec.	15.7%	3.3%	8.2%
$\alpha = 85°$, off-axis beam	18.4%	4.3%	9.8%
$\alpha = 90°$, on-axis beam	44.8%	5.0%	20.5%

Table 1: Averaged module of the relative increase of the square root of the noise angular power spectrum with respect of the case of pure white noise after applying the destriping algorithm (see also the text).

First of all from these simulations it seems that moving the spin-axis away from the ecliptic plane does not significantly help the destriping efficiency for typical LFI beam locations and, concerning the $1/f$ noise alone as source of drifts, it would be preferable to keep the spin-axis always on the Ecliptic plane. This is due to the off-axis position of most of the LFI beams, located at angles from about 2 to 6 degrees from the optical axis, according to the telescope size, the FPU configuration and the considered horn.

Furthermore for most of the LFI beams the choice of an angle $\alpha = 90°$ between the spin axis and the telescope axis would be acceptable: the destriping left only $\lesssim 2\%$ of excess noise with respect to the pure white noise case. On the other hand, some LFI beams are equivalent to on-axis beam which is clearly a degenerate case. A smaller value of α (namely 85°) breaks this degeneracy at an acceptable level yielding the usual destriping efficiency. From these two points an indication of a possible choice of the scanning strategy and instrument configuration arises: with $\alpha = 85°$ and precession of the spin-axis (no thermal drifts) with only 5° amplitude (half of what we considered here) appears satisfactory for de-striping performances while preserving full-sky coverage for all channels. This allows data redundancy but introduces irregularities in the integration time distribution, which may be an issue for the data analysis (see Fig. 3). Without spin axis modulations, a quite complete sky coverage and a smooth

integration time distribution at each frequency can be achieved only by assembling data from different receivers, losing redundancy.

The whole set of simulations seems to indicate that there is enough redundancy of observations to remove at acceptable level the contamination due to $1/f$ noise even if we require a more strict condition of crossings between scan circles (in the above results we have extracted the crossings when the pointings are inside the same map pixel with size of 13.7′). Of course, the performance of this destriping code could be partially optimized in the future by appropriately choosing the number of levels per circle and the crossing condition according to the dominant kind of instrumental noise (the parameters f_k and β), the magnitude of the gradients in the sky emission and our knowledge of other contamination sources.

For what concerns properly the $1/f$ noise, an important indication comes from the simulation with $f_k = 0.01$ Hz: the excess of noise before destriping reduces by a factor $\simeq 4 \div 5$ with respect to the case $f_k = 0.05$ Hz, indicating a possible linear relation between the additional *rms* and knee-frequency. In addition the extra noise level after destriping decreases, at least under these ideal assumptions, by a factor $\simeq 3$. The source of this extra noise after destriping is probably partially due to the $1/f$ noise on time-scales less than the spin-rate. This can be see when comparing the level of extra noise, after destriping, for the $f_k = 0.05$ Hz and $f_k = 0.01$ Hz cases, values larger and smaller than f_s respectively.

3 Recent developments on main beam distortion effects

The impact of main beam distortions introduced by optical aberrations on Planck measurements of microwave sky fluctuations has been carefully studied in several works (e.g. Burigana et al.. 1998a,b, Mandolesi et al. 1997, 1999b). It is clear that they may reduce the nominal angular resolution of the optical system, then degrading our capability of studying the high multipole range of CMB fluctuations, and make the measured antenna temperature dependent on the detailed beam shape and orientation, then introducing an additional systematic noise in the data at a level of some μK in terms of rms value.

As shown in Burigana et al. (1998a), at high galactic latitudes the combined effect of main beam distortions and of Galaxy emission fluctuations increases the added error at ~ 30 GHz by about 3 times with respect to the case of a pure CMB fluctuation sky, whereas it produces only a very small additional effect in the cosmological channels. In addition, the combined effect of beam distortions and extragalactic source fluctuations is found to be very small at all LFI frequencies (Burigana et al. 1999) compared to the noise induce by beam distortions in the case of a pure CMB sky. Then, it is enough to focus here further on the impact of the main beam distortions on the determination of angular power spectrum of CMB fluctuations by considering the idealized case of a pure CMB fluctuation sky (we consider here a typical standard CDM model, approximately COBE normalized).

The kind and the magnitude of optical distortions depend on the considered optical design; for aplanatic configurations (e.g. Villa et al. 1998 and Mandolesi et al. 1999a) the typical main beam shape is close to be elliptical owing to the strong reduction of spherical aberration and coma (see Fig. 4). Burigana et al. (1998a) provided simple approximations for the rms noise introduced by elliptical gaussian beams. It should be noted that the present telescope design (called Alcatel "Case 1") is based on an aplanatic solution.

We have recently improved our analysis by understanding also what range of multipoles is mainly affected by beam distortions, by resorting to detailed extensive simulations.

We have computed here a full year reduced version simulation both for a pure symmetric gaussian beam with FWHM $= 2\sqrt{2\ln 2}\sigma = 30'$ and for an elliptical gaussian beam with axial

ratio $r = 1.3$ and with the same effective resolution ($\sqrt{\sigma_x \sigma_y} = \sigma$) of the considered symmetric beam ($r = 1$): we shift the spin axis at steps of $5'$ and consider a step of $10'$ between two samplings on the same scan circle (this simplification does not prevent the understanding of the main results, being the sky significantly oversampled inside the beam size). We computed the difference between the maps obtained with the elliptical and the symmetric beam by coadding the corresponding data streams and calculate the angular power spectrum of this difference map. This provides an estimate of the error introduced by main beam distortions on the determination of CMB angular power spectrum, in absence of appropriate deconvolution techniques able to take accurately into account the main beam detailed shape, owing for example to uncertainties in its reconstruction. As shown in Fig. 5, this effect is particularly relevant at quite large multipoles, close to the CMB peak (where the Galaxy straylight contamination power drops out, see next section); the magnitude is clearly related to the value of r.

From optical simulations we know that r typically increases with the distance from the beam centre. From the present simulations we infer that a value of r quite smaller than 1.3, say less than $\simeq 1.1$ up to -3 dB from the centre and less than $\simeq 1.2$ up to -20 dB from the centre, is good enough for avoiding significant contaminations in the data, in agreement with the indications inferred on the basis of the approximations of Burigana et al. (1998a) for the rms added noise.

4 On Galaxy straylight contamination

The straylight contamination due to Galaxy emission (GSC) entering at large angles from antenna pointing direction may be one of the most relevant sources of systematic effects in Planck observations of the cosmic microwave background (CMB) anisotropies.

Since the antenna response features at large angular scales from the beam centre (far sidelobes) are determined largely by diffraction and scattering from the edges of the mirrors and from nearby supporting structures, they can be reduced by reducing the illumination of the edge of the primary, or in the jargon of antenna design, increasing the edge taper, defined as the ratio of the power per unit area incident on the center of the mirror to that incident on the edge. Of course, lower is the edge taper and lower is the sidelobe level; on the other hand lowering the edge taper has a negative impact on the angular resolution (e.g. Mandolesi et al. 1999b). A trade off between angular resolution and straylight contamination has to be found.

The main astrophysical source of straylight at the LFI channels derives from the Galactic emission and depends on the observed sky region, on the frequency and on the shielding efficiency. At the LFI frequencies, the Galaxy straylight contamination (GSC) is expected to be particularly crucial at the lowest frequency channels, due to the increasing of synchrotron emission and anisotropies with the wavelength.

On the basis of the antenna integrated response from angular regions at different distance from the beam centre and of the level of Galaxy emission we can provide simple estimates of the expected GSC.

We have considered the old Planck Carrier configuration studied by De Maagt et al. (1998) with $\alpha = 80°$ and including shields; we remind the reader to that document for further optical details. We have considered the antenna pattern at 30 GHz with the beam centre located at $\theta_B = 5.62° g$ and $\phi_B = 126.03°$ in the telescope frame (see Fig. 6). It should be noted that the average behaviour of the GSC does not strongly depend of the telescope design.

Of course detailed and precise GSC maps should be computed for the actual telescope plus shield configuration.

We can distinguish among pattern regions at different angular distance θ from the beam centre. The region with θ between $\simeq 1.2°$ and $\simeq 2°$ contains about the 0.5% of the integrated response, the ~ 0.6 % being contained in the region between $\simeq 1.2°$ and $\simeq 5°$, and the $\simeq 1$ % at $\theta \gtrsim 5°$; of course the remaining main integrated response falls in the "main" beam (up to $\simeq 1.2°$). In addition, in the main spillover enters $\approx 0.1 \div 0.2\%$ of the integrated response.

For the present numerical estimates, performed at 30 GHz, the relevant astrophysical source is the Galaxy emission, known at a resolution of of about 2.5° by COBE-DMR. We have implemented "small" angular extrapolations (see e.g. Burigana et al. 1999 for further details) for generating Galaxy maps with resolution of about 1°.

For simple estimates, we note that in the adopted 30 GHz Galaxy map there are $\sim 13\mathrm{deg}^2$ with a signal (in terms of antenna temperature T_a) larger the 2 mK, $\sim 73\mathrm{deg}^2$ with $T_a > 1.5$ mK and $\sim 230\mathrm{deg}^2$ with $T_a > 1$ mK, while the minimum signal is ~ 0.05 mK and about the 50% of the sky shows a signal ~ 0.1 mK.

By combining these numbers with the percentages of integrated responses falling within the above different angles from the beam centre, we expect to find a contamination peaking at about 10 μK from the pattern regions between $\simeq 1.2°$ and $\simeq 5°$ and at some μK from the pattern regions outer than $\simeq 5°$. In particular, in the main spillover we expect a signal peaking at ~ 2 μK when it looks at high signal galactic regions. Contributions of the some level are expected from the pattern features at few tens of degrees from the beam centre. Of course, smaller contaminations ($\sim 0.5\mu$K) are expected when the relevant features look at low signal galactic regions.

Numerical calculations are required for more accurate estimates. We have implemented our simulation code of Planck observations by including the convolution of the full sky with the full antenna pattern by working in real space [see Wandelt & Górski (1999) for a discussion on the pattern full sky convolution by working in the spherical harmonic space and using the Wigner matrices for rotating spherical harmonic expansion coefficients, a method which allows to reach high accuracy with a significant computational time saving due to the reduction of the spherical harmonic expansion to Fast Fourier Transforms].

We compute separately the absolute signals from three reference pattern regions: the main beam (at $\theta \leq 1.2°$), the intermediate beam (at $1.2° \leq \theta \leq 5°$) and far pattern (at $\theta \geq 5°$). For the 30 GHz channel, the pattern region outside $\simeq 1.2°$ corresponds to antenna responses lower than $\simeq -40$ dB with respect to the peak response, where the beam response probably becames highly difficult to measure in flight through planets (Mandolesi et al. 1998); $\theta \simeq 5°$ approximately divides pattern regions where significant response variations occur on angular scales much less than 1° from those where they occur on $\sim$ degree or much larger scales.

We have studied the impact of GSC on Planck observations at 30 GHz, by considering different and complementary evaluation approaches: absolute and relative quantification of the impact on scan circle data streams, Fourier decomposition of scan circle signal, computation of maps of GSC and evaluation of their angular power spectrum. These different methods allow us to focus on different aspects of GSC.

All simulated data streams for a 1 yr mission (in "roughly" ecliptic coordinates, properly the spin axis longitude and a reference angle along the scan circle) are synthetically reported in Fig. 7.

Note that the signal entering the intermediate pattern is approximately proportional to that in the main beam: two relative maxima typically appear, related to the two crossings of the galactic plane. The signal from outer pattern regions exhibits a clearly different and

shifted angular pattern: more or less, four relative maxima are present, two introduced by the main spillover and two by features closer to the main beam, as they cross the galactic plane.

In the central panel, note the features close to the galactic plane, mainly produced by the pattern features not very far from the main beam. Note that the azimuthal asymmetry of the main spillover reflects in the large difference between the two halfs (along x axis) of the right panel of Fig. 7.

We have applied the Fourier serie decomposition to the sum of intermediate and far pattern (i.e. for $\theta \geq 1.2°$) data streams from some scan circles. The same decomposition has been applied to white noise data streams, computed according to the LFI sensitivity at 30 GHz averaged over a number of scan circles that spans an ecliptic longitude arc length equal to the FWHM $= 33'$, i.e. essentially the sensitivity corresponding to half year mission. The white noise power is above that of the signal entering at $\theta \geq 1.2°$, for practically all the modes $m \gtrsim 3$, becaming ≈ 10 larger at $m \approx 10$; this is essentially due to the strong decreasing of Galaxy fluctuations at small angular scales.

By coadding the data streams we can obtain the corresponding maps.

The map from intermediate pattern is approximately proportional to that derived from the main pattern with an intensity scaled by the fraction of integrated response entering the the corresponding portion of antenna pattern. On the contrary, the sky "observed" by the far pattern is very different. The signal is higher close to the galactic plane, because of the features in the antenna pattern within $10° - 20°$ from the main beam, and at about 90° from the galactic plane, because of the signal entering the main spillover.

We can compute the angular power spectra of the GSC maps (Fig. 8) and compare them with the angular power spectrum of the white noise for four and a single 30 GHz receiver (dotted lines) and with the CMB anisotropy angular power spectrum (a tilted - $n_p = 0.9$ - power spectrum with standard CDM cosmological parameters and approximately COBE normalized is reported here, thick solid line) and with that of Galaxy fluctuations (dot-dashed lines), as seen by the main pattern (upper line: without map cuts; lower line: by considering only the regions at $|b| \geq 30°$). We show separately the contribution from intermediate (solid green line) and far (solid red line) pattern regions. The most important contamination in terms of angular power spectrum derives from the signal intermediate pattern when all the sky is considered; on the contrary, considering only the regions at $|b| \geq 30°$ (dashed lines: green for the intermediate pattern, red for the far pattern) the GSC power spectrum is dominated by the far sidelobes (red dashed line). In general, this effect is relevant at low multipoles and becames less than 20 times smaller than white noise power spectrum at $l \simeq 50$, due to the decreasing of Galaxy fluctuation spectrum at high multipoles.

We find that the GSC affects the determination of CMB angular power spectrum at large multipoles significantly less than other classes of instrumental effects, like main beam distortions and $1/f$ noise. On the other hand, although the GSC global effect is largest at low galactic latitudes, the contamination (peaking at $\sim 6\mu$K) produced by far pattern features at intermediate and high galactic latitudes may be crucial, being there minimum the Galaxy contamination and extremely good the nominal Planck sensitivity, allowing also for accurate polarization measurements.

Our simulations show that the GSC peaks at values of $\simeq 15\mu$K, a value comparable with the sensitivity per pixel, owing to the signal entering at few degrees from the beam centre; it occurs in the regions close to the galactic plane where in any case the "direct" (i.e. observed by the main beam) contamination from the Galaxy prevents an accurate determination of CMB fluctuations, being not trivial the subtraction of Galaxy emission at levels less than

few % accuracy. These large contamination values, although critical for CMB anisotropy measurements, are not crucial for the determination of Galaxy emission, which is several order of magnitude larger. In general, the typical value of GSC is less than the 50% of the white noise sensitivity.

The most crucial contamination for the Planck goal is that introduced by far pattern features, the corresponding signal peaking at $\simeq 6\mu$K; this contamination, although smaller than that from intermediate pattern regions in terms of absolute values, dominates the GSC at high galactic latitudes where we can extract the maximum informations on CMB fluctuations. In terms of both angular power spectrum and added rms noise these values are not particularly crucial, being less (but not too much) than the rms sensitivity.

This systematic effect, which could affect mainly the determination of the low multipole part of the CMB angular power spectrum, is not so crucial compared to other instrumental effects, main beam distortions and $1/f$ noise, that affect the determination of CMB angular power spectrum al large multipoles. Nevertheless the contribution to the noise introduced by beam distortion from inner pattern regions can be in principle subtracted if the beam pattern is accurately known there. On the other hand we have to keep in mind that currently the reduction algorithms have been not tested for all the systematic (instrumental & astrophysical) together.

In spite of this quite optimistic general considerations, we stress here some critical aspects derived from our analysis. The two quite wide regions close to the ecliptic poles where Planck sensitivity is several times better than the average, are the regions where, according to the detailed location orientation of the ensamble of beams, the GSC from far pattern peaks. Then it is not true that locally the GSC is smaller than the sensitivity. This issue may be particular crucial for polarization measurements that take maximum advantage from the highest sensitivity regions. In this respect, the conclusions on GSC impact are not so optimistic as delined above and lower values of GSC have be achieved for avoiding significant systematic contaminations in the two high sensitivity patches.

From the analysis of the GSC in the two six months, one could be simplicistically infer that the worst case GSC could be thrown away in favor of the less contaminated one. But this is particularly dangerous for: safety reasons, redundancy reasons and because a good subtraction of GSC take advantage from high sensitivity which is reduced if one has to work with half data only.

Of course it is important to analyze the impact of Galaxy straylight for the whole set of Planck antennas in the more updated version of the payload for fully understanding the GSC impact on LFI science; the cosmological channels will be clearly less contaminated by this effect, nevertheless it is clear that, in particular for the patches at highest sensitivity, the cosmological information will be much better as long as we can accurately control foregrounds and their coupling with instrumental effects at low frequency.

5 On the coupling between $1/f$ noise and optical distortions

We have implemented our simulation code for studying the combined effect of $1/f$ noise and main beam distortions. In Fig. 9 we show the angular power spectrum of receiver noise before and after applying the destriping algorithm when we include also a main beam elliptical distortion with $r = 1.3$ for a beam with FWHM=30′ and located at $\theta_B = 2.8°$, $\phi_B = 45°$ for a simple scanning strategy with $\alpha = 90°$, a "mean" location for what concern the destriping efficiency (Maino et al. 1999). As evident the quality of destriping algorithm is not significantly affected by the additional uncertainty introduced by the "systematic"

differences among the observed temperatures resulting from different orientations of the main beam at the crossing points of different scan circles.

So far, we find a crucial difference between GSC, main beam distortion induced noise and $1/f$ noise. The GSC affects particularly the determination of CMB angular power spectrum at low multipoles, whereas main beam distortions are critical at large multipoles; $1/f$ noise affect both high and low multipoles, but the proposed destriping algorithm is particularly efficient in removing high multipole blobs. It is clear that all these effects have to be reduced both via hardware and software. $1/f$ noise can be reduced independently of the other two, its magnitude being related essentially to the cooling efficiency and to the scanning strategy: the 4 K option for the reference load allows to significantly reduce also low multipole contamination (Maino et al. 1999). Because the GSC and beam distortions are related mainly to the optical design, their effect have to be optimised by chosing an appropriate feed and telescope designs, as discussed in Mandolesi et al. (1999b). Unfortunately, for a given telescope design, increasing the angular resolution has a negative impact on the GSC and viceversa, due to the fact that their relative weight is controlled by the feed illumination. We have to optimize the design to find a trade off for reducing the combined impact of both these effects.

6 Instrumental versus astrophysical contamination

The impact of foregrounds on the primary cosmological goal of Planck mission has been extensively studied in literature for what concern both galactic and extragalactic contaminations, of discrete and diffuse origin. On the other side, Planck itself is good opportunity for studying cluster physics, many classes of extragalactic and galactic sources and the diffuse emission from the Galaxy (De Zotti et al. 1999a). Many approaches have been studied to separate the different components of the microwave sky and for deriving their angular power spectra (e.g., Baccigalupi et al. (2000) and references therein).

The Galaxy angular power spectrum is known to decrease with the multipole: we show in Fig. 10 the power spectrum derived from the map observed by the adopted main pattern (thin dots-dashes) by cutting the region at $|b| \leq 30°$ and the power spectra proposed by Tegmark & Esftathiou (1996) for free-free (thick dots), synchrotron (upper thick dots-dashes) and dust (upper thick dashes) emission at relevant galactic latitudes. We show also for comparison the power spectra for synchrotron (lower thick dots-dashes) and dust (lower thick dashes) as derived by Prunet et al. (1998) and Bouchet et al. (1998) for a sky patch at intermediate latitudes. Of course, Galaxy contamination strongly depends on the considered region.

Microwave fluctuations from extragalactic unresolved discrete sources are dominated by the Poisson contribution and then increase in terms of δT approximately proportionally to the multipole ℓ. We show in Fig. 10, separately for radiosources (thin solid lines) and far infrared galaxies (thin dashes), the Poisson fluctuation power spectra predicted by Toffolatti et al. (1998) as improved by De Zotti & Toffolatti (1999), Toffolatti et al. (1999) and De Zotti et al. (1999b) on the basis of current source counts and assuming evolution models and spectra in agreement with current data, when sources above 1 Jy (upper curves) or 100 mJy (lower curves) are detected and subtracted. Of course radiosources dominate at low frequencies. We have taken into account here a gaussian (FWHM=33′) beam smoothing in all cosmological and astrophysical angular power spectra and consequently neglected it in the receiver noise angular power spectrum.

At low multipoles, Galaxy contamination is larger then instrumental effects, dominated by the GSC (and the residual $1/f$ noise in absence of very efficient cooling); on the other hand, if Galaxy emission and anisotropy can be modelled at few percent accuracy and at

high galactic latitudes instrumental effects can became comparable with Galaxy unsubtracted contamination.

At high multipoles, main beam distortions may introduce an additional noise comparable with that from radiosource fluctuations, if we are able to subtract them at few hundreds mJy level and the telescope is not optimized for reducing optical distortions and not well tested deconvolution methods for subtracting them are available.

7 Conclusions

We have discussed the impact of three classes of instrumental effects on Planck LFI observations taking into account the most relevant informations on the instrumental performances currently available. A detailed simulation work is crucial to optimize the design of Planck mission, to achieve the scientific goals and prepare the data processing work.

In the next future we have to devote strong efforts to accurately simulate the Planck observations to be able to take together into account a wide collection of both instrumental and astrophysical effects for the full set of Planck LFI detectors in the payload, telescope and instrumental updated version.

References

[1] Baccigalupi, C. et al., 2000, MNRAS, submitted, astro-ph/0002257

[2] Bersanelli, M. et al., 1996, ESA, COBRAS/SAMBA Report on the Phase A Study, D/SCI(96)3

[3] Bouchet, F.R., Prunet, S. & Sethi, S.K., 1999, MNRAS, 133, 663

[4] Burigana, C. et al., 1997, Int. Rep. TeSRE/CNR 198/1997, astro-ph/9906360

[5] Burigana, C. et al., 1998a, A&ASS, 130, 551

[6] Burigana, C. et al., 1998b, Proceedings of *XXXIIIrd Rencontres de Moriond - "Fundamental Parameters in Cosmology"*, Eds. J. Tran Thanh Van et al., pg. 171–174.

[7] Burigana, C. et al., 1999, Astro. Lett. Comm. in press, astro-ph/9903137

[8] Coolet, J.W. & Tukey, J.W., 1965, "An algorithm for machine calculation of complex Fourier series", Math. Computat., vol. 19, 297

[9] De Maagt, P., Polegre, A.M. & Crone, G., 1998, Planck - Straylight Evaluation of the Carrier Configuration, Technical Report ESA, PT-TN-05967, 1/0

[10] De Zotti, G. & Toffolatti, L., 1999, Astro. Lett. Comm. in press, astro-ph/9812069

[11] De Zotti, G. et al., 1999, Proceedings of the EC-TMR Conference "3 K Cosmology", Roma, Italy, 5-10 October 1998, AIP Conference Proc. 476, Maiani, L., Melchiorri, F. & Vittorio, N., (Eds.), pg. 204, astro-ph/9902103

[12] De Zotti, G. et al., 1999b, New Astronomy, 4, 481

[13] Gaier, T. et al., 1996, SPIE Proceedings, Millimeter and Sub-millimeter III, 2842, 46

[14] Heideman, M.T., Johnson, D.H. & Burrus, C.S., 1984, "Gauss and the history of the FFT", IEEE Acoustics, Speech and Signal Processing Magazine, Vol.1, 14

[15] Janssen, M. et al., 1996, astro-ph/9602009

[16] LFI Design Report, Planck Low Frequency Instrument, Instrument Science Verification Review, October 1999

[17] Maino, D. et al., 1999, A&ASS, 140, 1

[18] Mandolesi, N. et al., 1997, Int. Rep. TeSRE/CNR 199/1997

[19] Mandolesi, N. et al., 1998, Planck LFI, A Proposal Submitted to the ESA

[20] Mandolesi, N. et al., 1999a, Astro. Lett. Comm. in press, astro-ph/9904135

[21] Mandolesi, N. et al., 1999b, A&A, submitted

[22] Prunet, S. et al. 1998, A&A 339, 187

[23] Seiffert, M. et al., 1997, Rev. Sci. Instrum, submitted

[24] Tegmark, M. & Efstathiou, G., 1996, MNRAS 281, 1297

[25] Toffolatti, L. et al., 1998, MNRAS 297, 117

[26] Villa, F., Mandolesi, N. & Burigana, C., Int. Rep. TeSRE/CNR 221/1998

[27] Wandelt, B.D. & Górski, K.M., 1999, "A Preliminary Study of Sky Observations with the PLANCK Surveyor Satellite", http://www.tac.dk/wandelt/papers.html

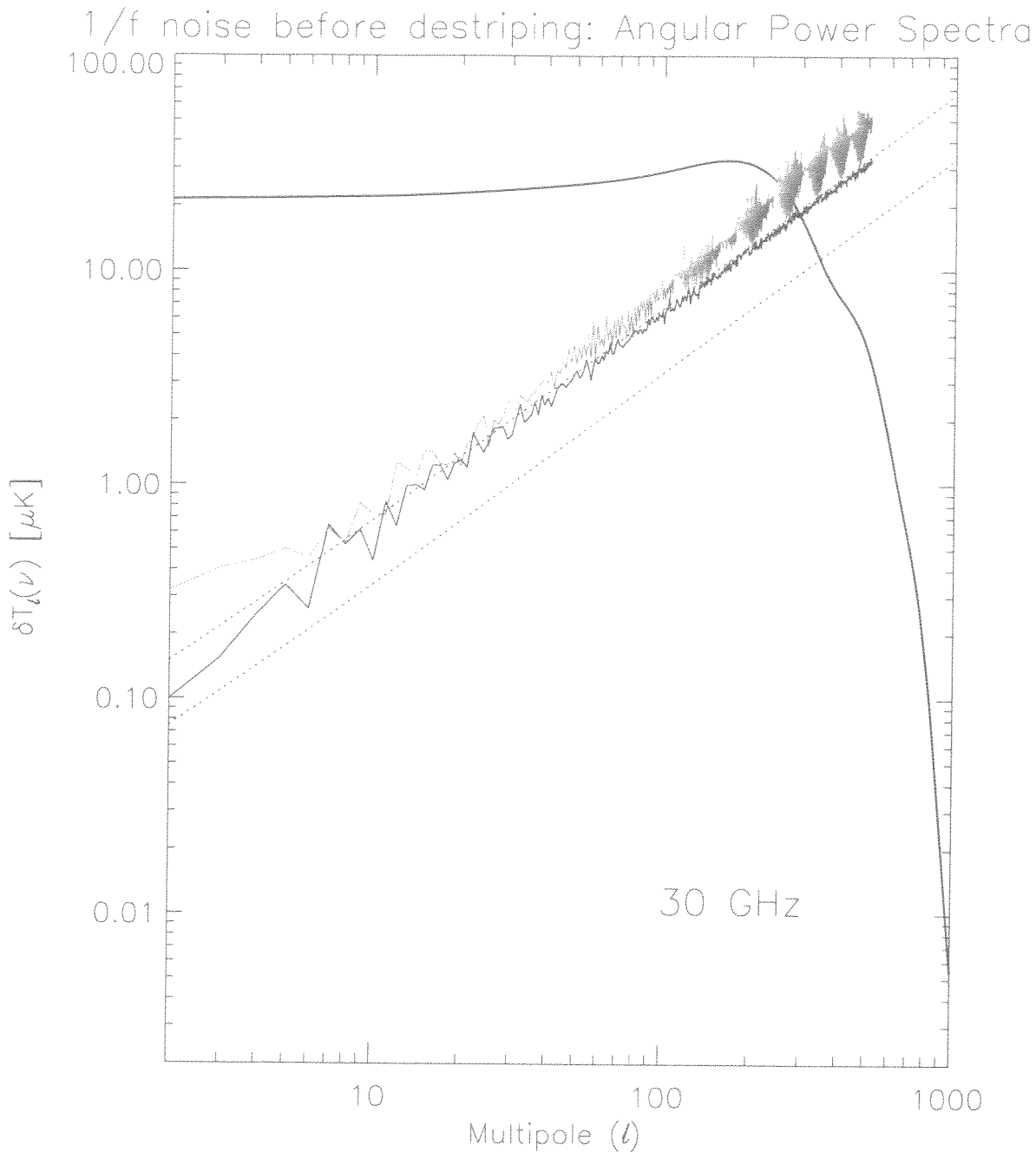

Figure 1: Noise power spectra at 30GHz before destriping (red line). Simulations parameters are: $\alpha = 90°$, $(\theta_B, \phi_B) = (2.8°, 45°)$, $f_k = 0.05$ Hz and spin-axis always on the Ecliptic plane. The white noise spectrum and its theoretical level (for one and four receivers, dots) are also reported for comparison (black lines). The excess of noise is about 40% over the white noise level. We report also the CMB power spectrum for a standard CDM model convolved with a gaussian beam with FWHM=30′ (thick black solid line).

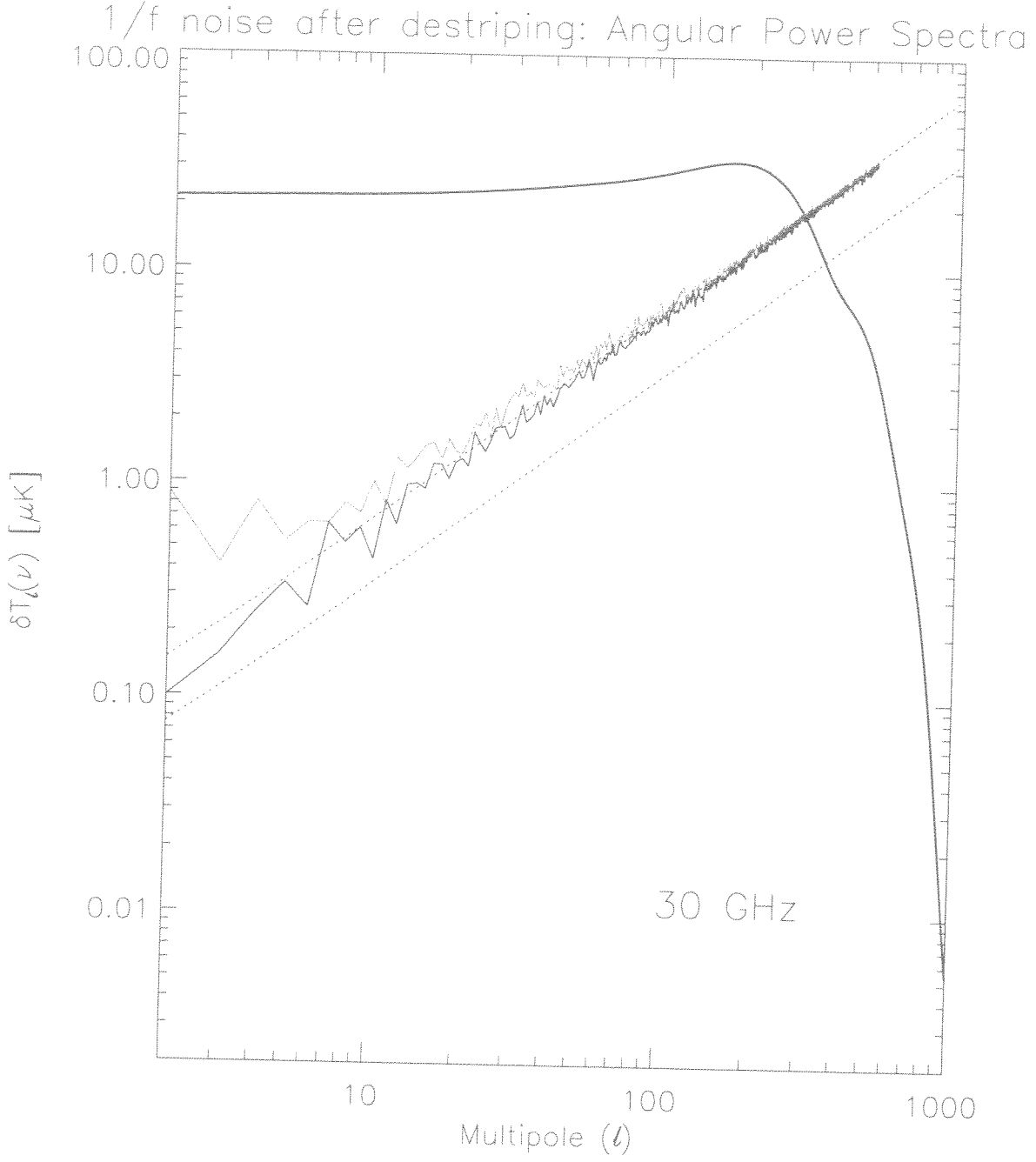

Figure 2: The same as in Fig. 1 but after destriping (green line). Now the added noise is only 1-2% of the white noise level.

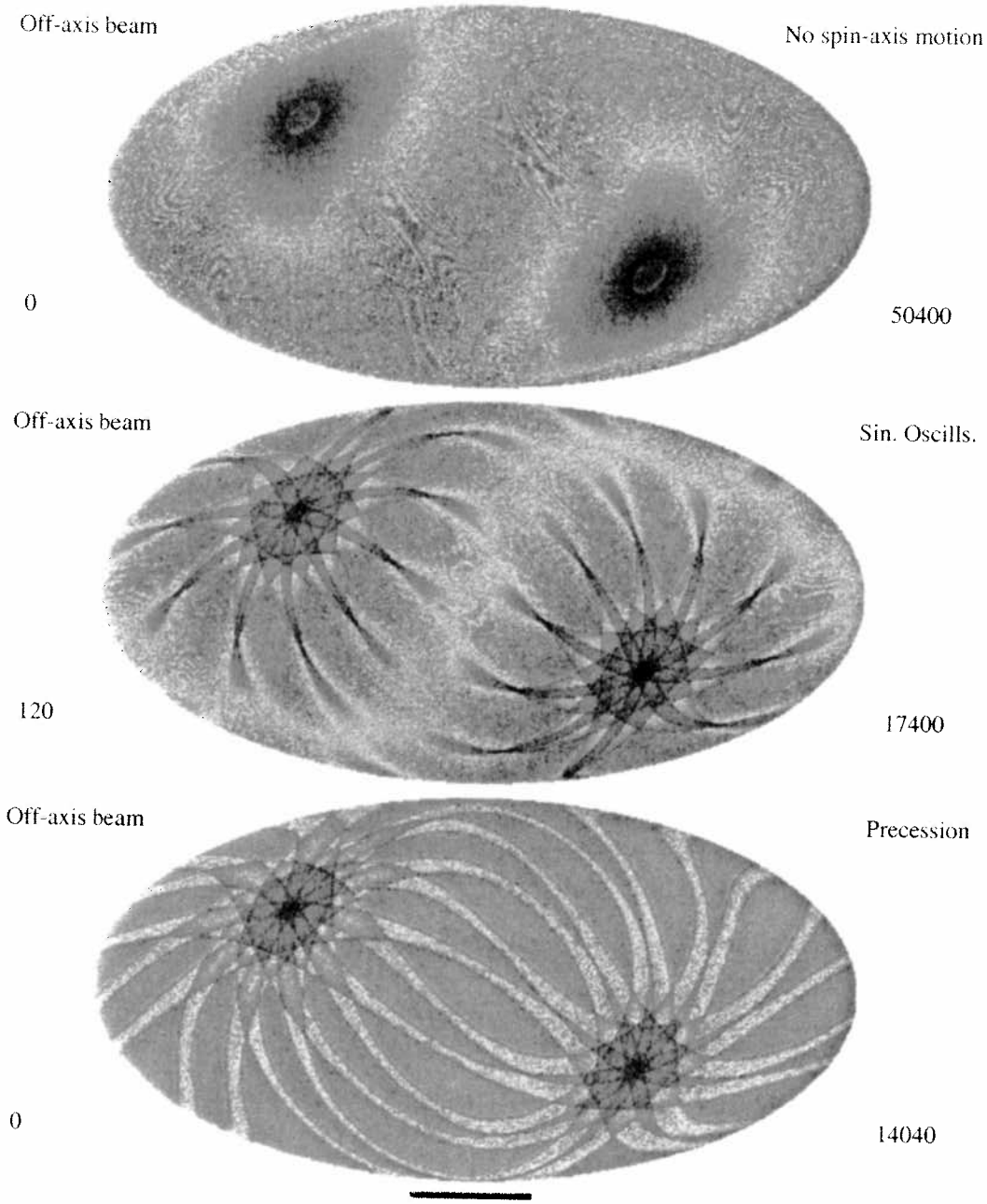

Figure 3: Distribution in the sky of the number of observations per pixel for three different scanning strategies and 1 yr of observation. We have considered here a typical LFI off-axis beam, $(\theta_B, \phi_B) = (2.8^\circ, 45^\circ)$, and an angle $\alpha = 85^\circ$ between the spin axis and the telescope optical axis. We show here the case of 10 spin axis oscillations per year with an amplitude of $\pm 10^\circ$.

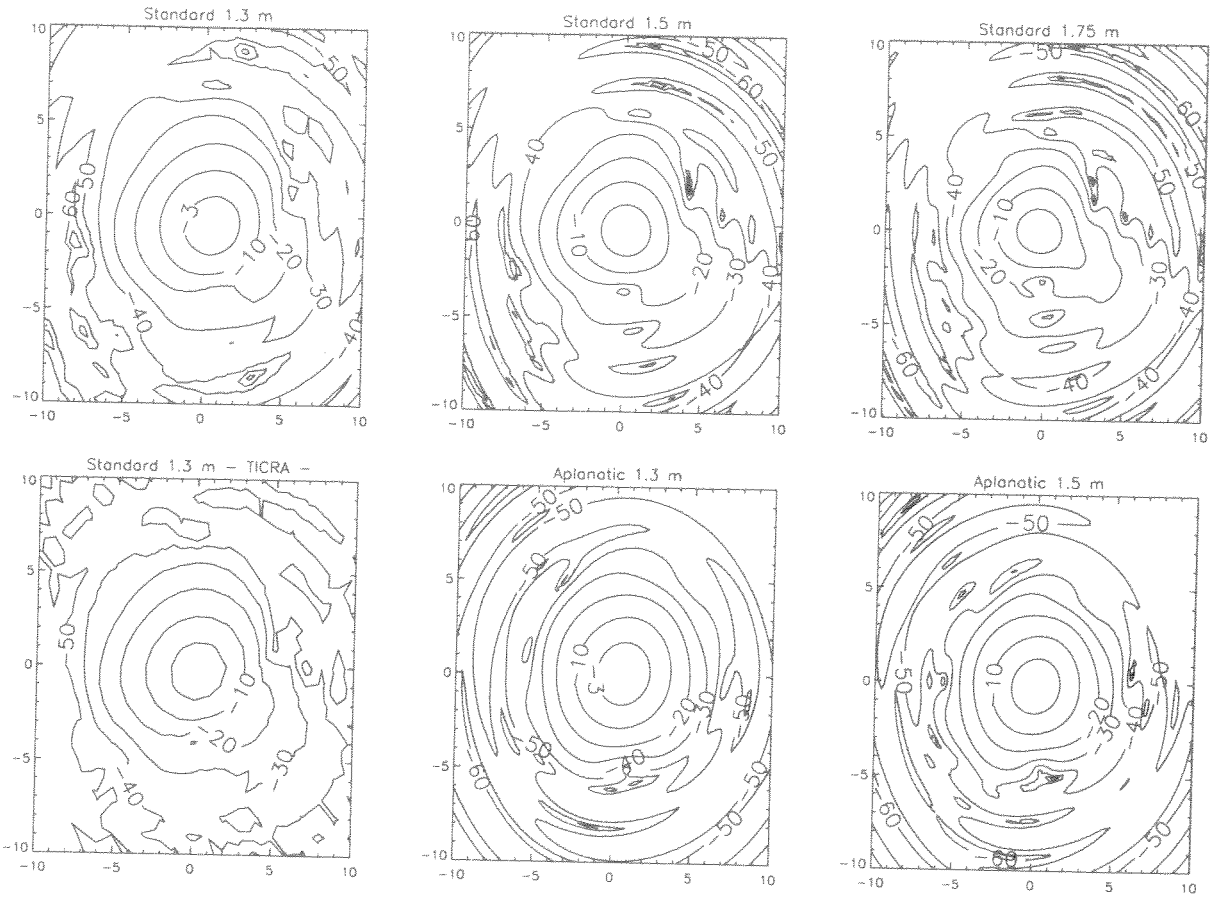

Figure 4: Contour plot of the normalized patterns of a beam located at El=+2°, Az=-2° from the optical axis for the optical (labelled with "standard") design like that proposed for the PHASE A study (1.3 m aperture), for two analogous optical configurations but with primary aperture of 1.5 m and 1.75 m and for an aplanatic design with aperture of 1.3 m and 1.5 m, computed as in Villa et al. 1998 and Mandolesi et al. 1999a (for the 1.3 m "standard" telescope we show also the pattern computed by TICRA for comparison). In each panel, the x and y axes are the standard U and V coordinates in radians (multiplied by 1000) in a reference approximately translated to the beam center.

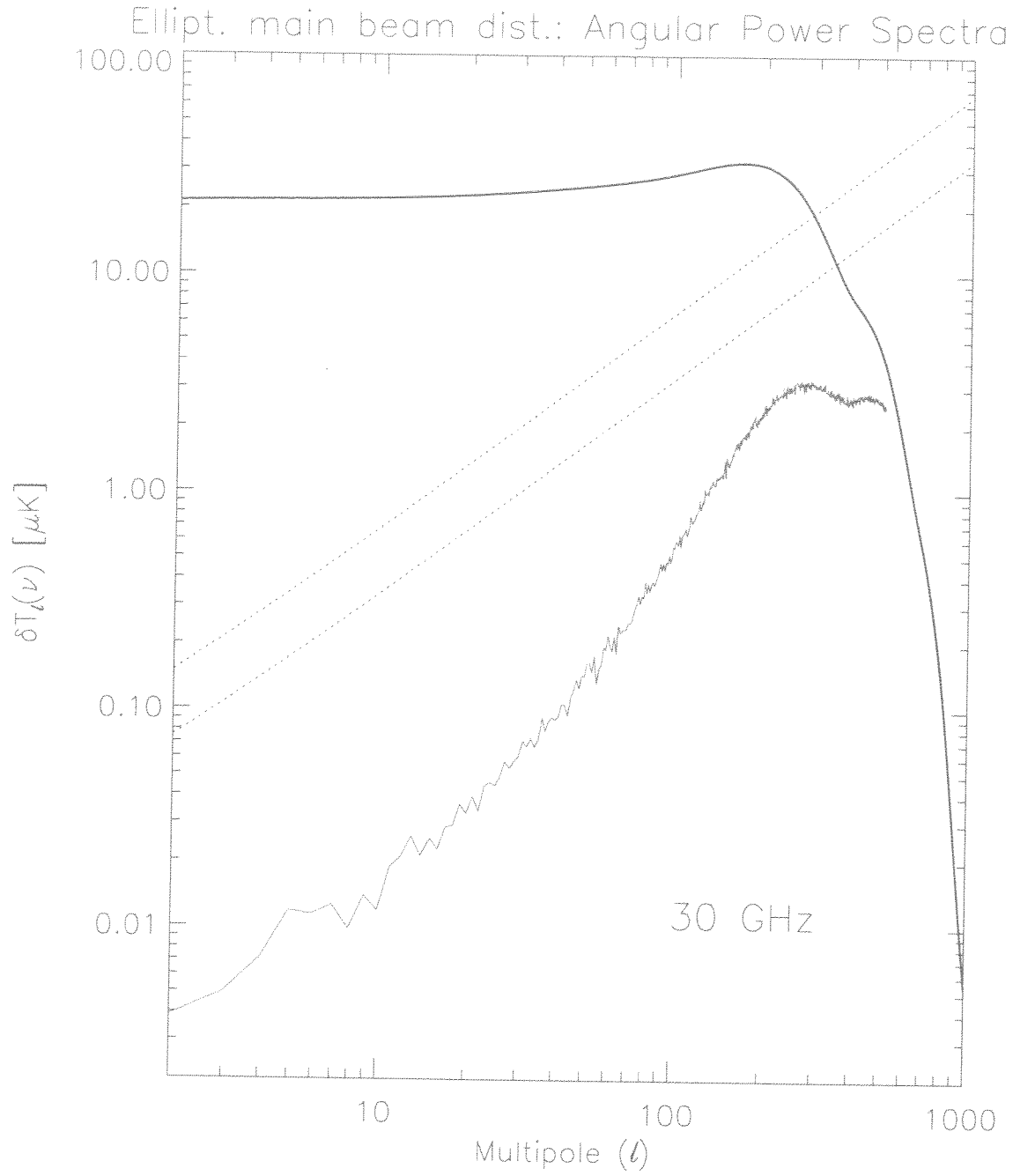

Figure 5: Angular power spectrum of the additional noise introduced by main beam distortions for a representative case of elliptical beam (blue line) compared to that of the pure white noise for a single 30 GHz receiver, for four 30 GHz and of the CMB. Note how large mutipoles, quite close to the CMB peak, are affected (see the text for further details).

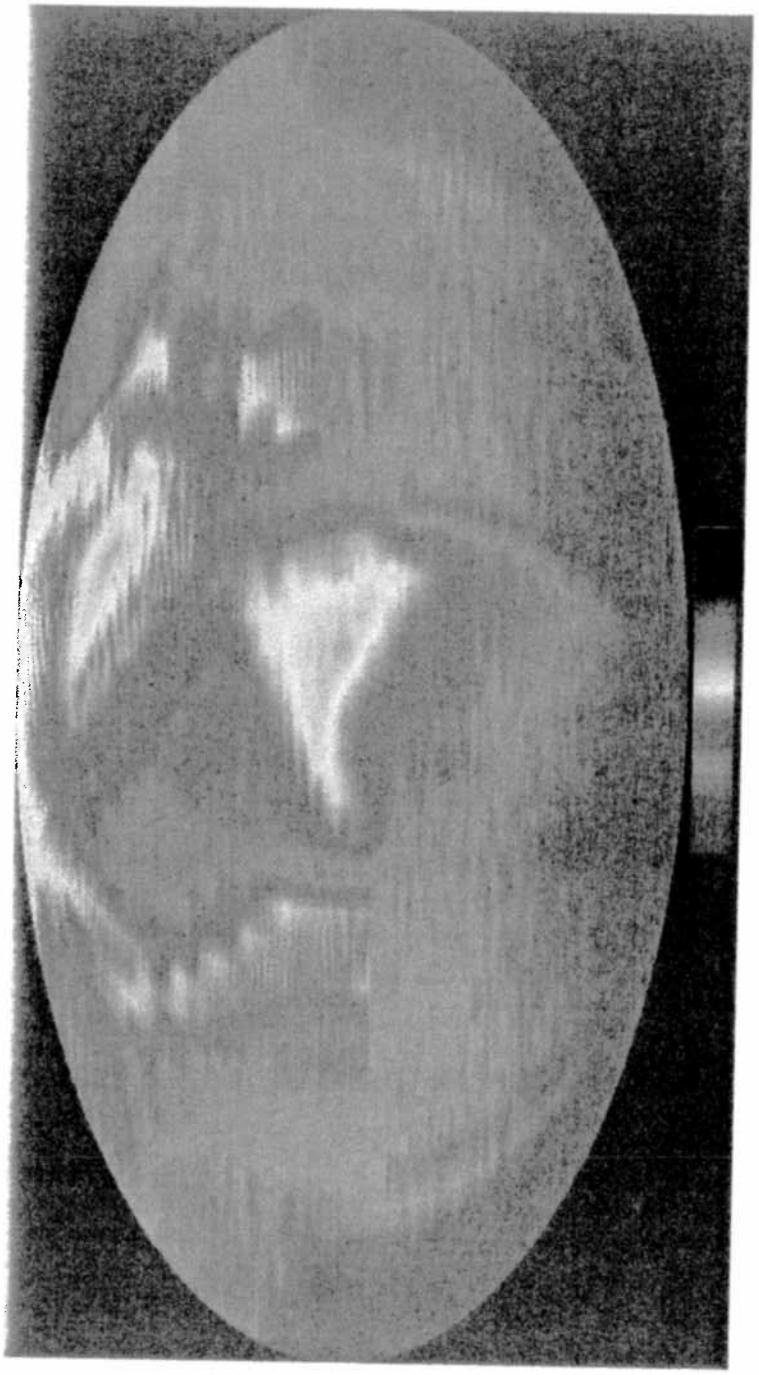

Figure 6: Full antenna pattern, with response normalized to the maximum, for the carrier configuration. The color table is linear in dB and the true directivity at the maximum is 49.36 dB. The pattern response at the main spillover peak (located close to the map center in this projection) is $\simeq 3 \times 10^{-6}$ the response at the main beam maximum.

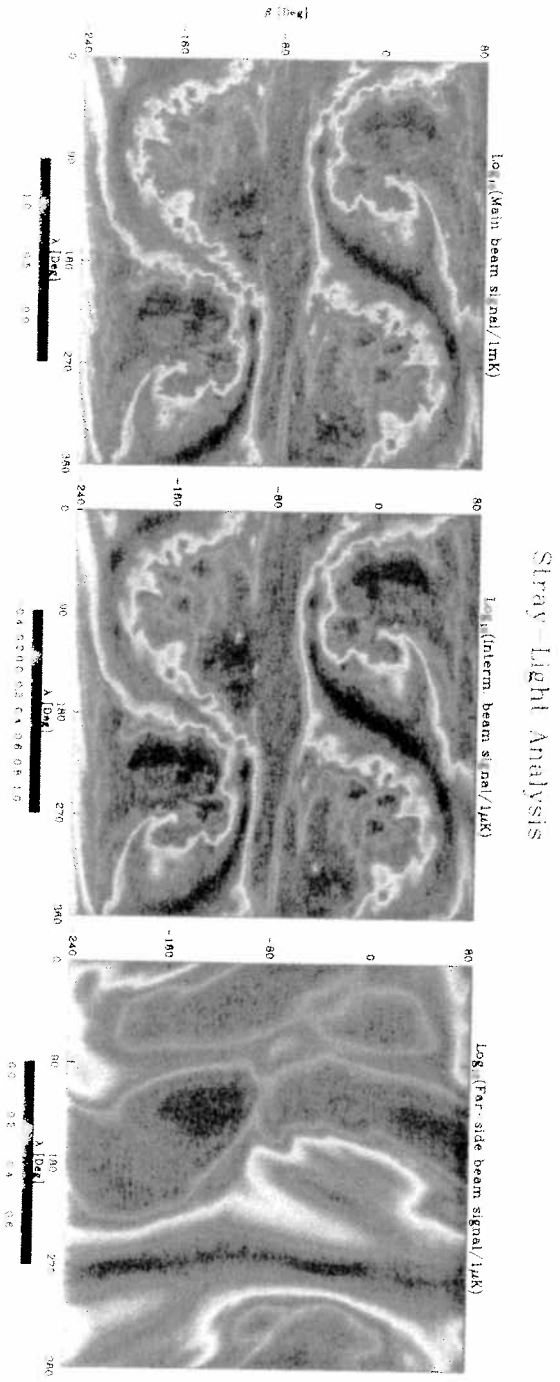

Figure 7: Synthetic view of the data stream from all scan circles for $\alpha = 80°$. The ecliptic coordinated λ and β properly refer here to the direction of the telescope axis (see the text for further details).

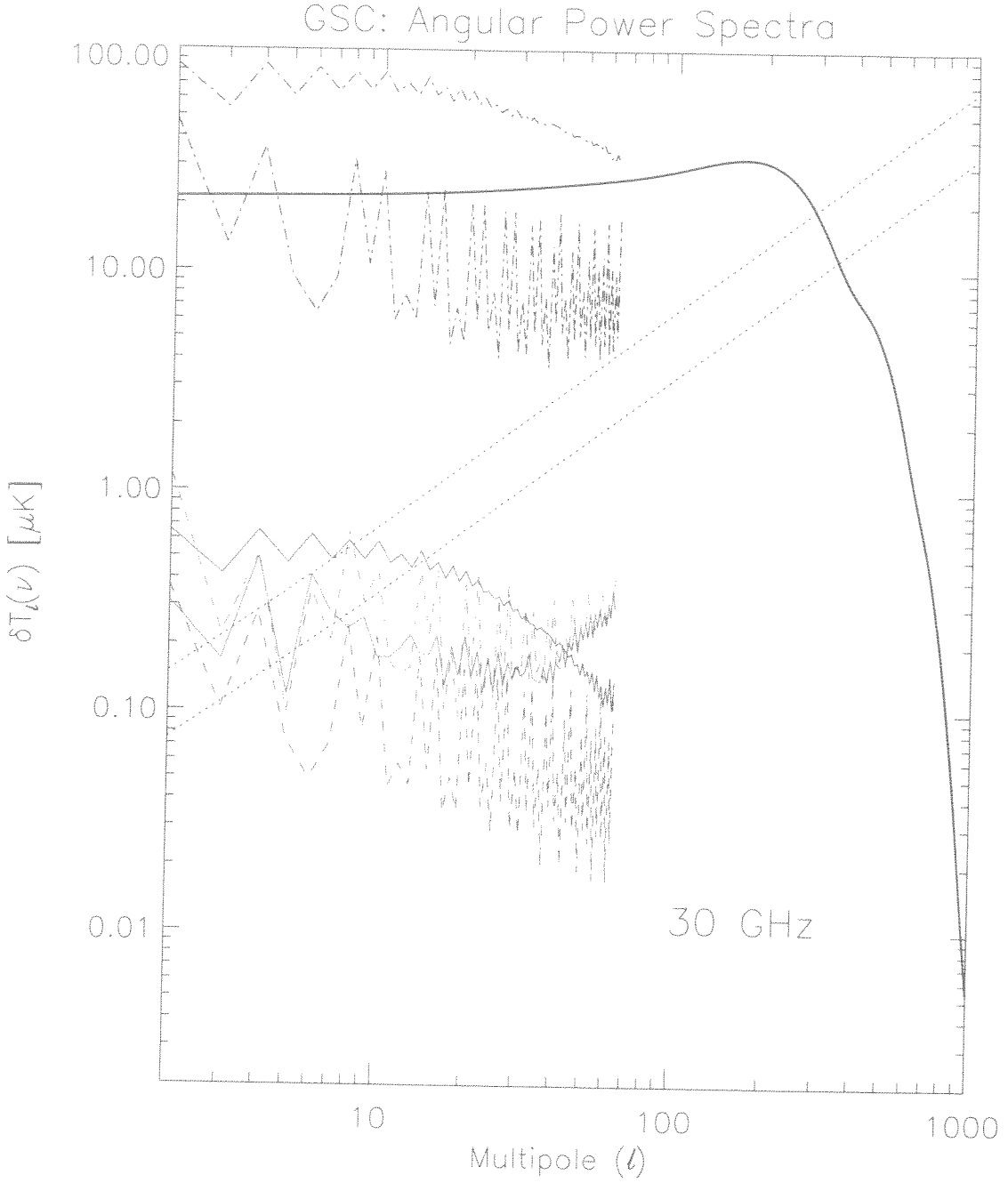

Figure 8: Comparison between GSC angular power spectrum from different pattern angular regions (see the text for further details and for the meaning of the different lines).

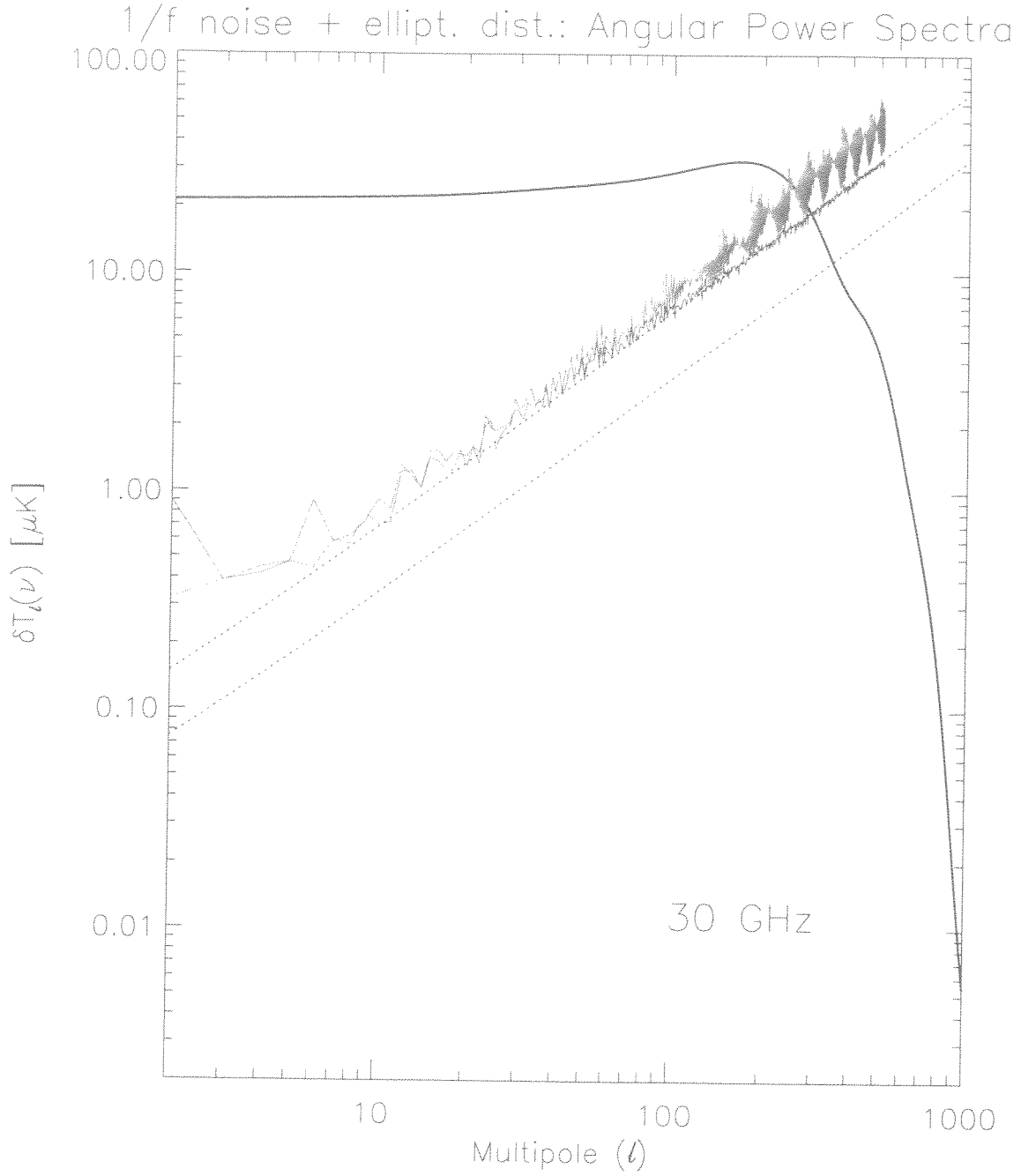

Figure 9: Angular power spectrum of receiver noise before (red line) and after (gren line) applying the destriping algorithm when we include also a main beam elliptical distortion with $r = 1.3$ for a beam with FWHM=30′ and located at $\theta_B = 2.8°$, $\phi_B = 45°$ for a simple scanning strategy with $\alpha = 90°$.

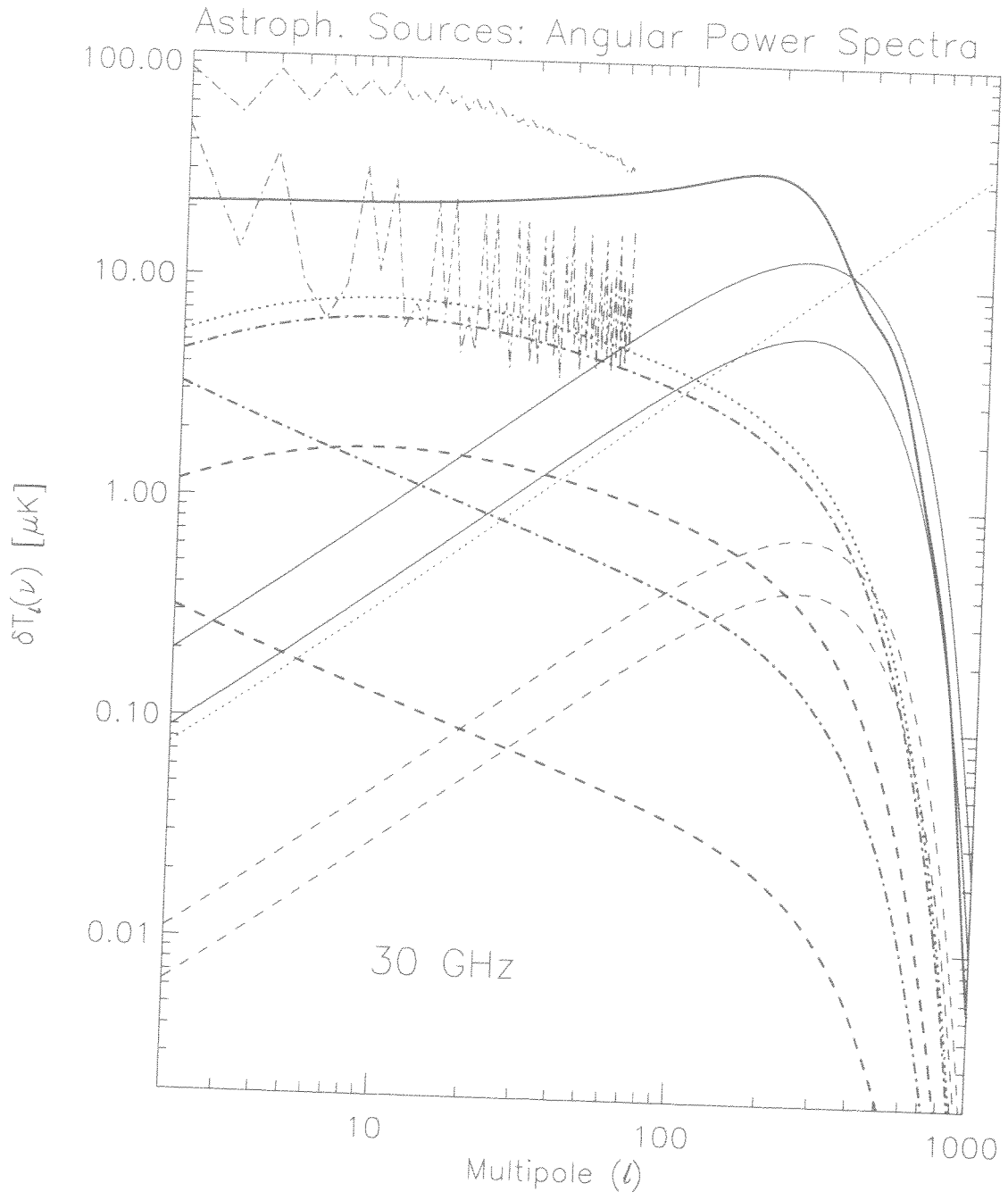

Figure 10: Angular power spectra of astrophysical foregrounds (see the text for further details and for the meaning of the different lines).